11-30-2010

# Substrate-Mediated Spreading and Phase Segregation at LSM-Zirconia Interfaces

Ju-Sik Kim
*University of Pennsylvania*

Shiwoo Lee
*University of Pennsylvania*

Raymond J. Gorte
*University of Pennsylvania*, gorte@seas.upenn.edu

John M. Vohs
*University of Pennsylvania*, vohs@seas.upenn.edu



Suggested Citation:
Kim, J.S., Lee, S., Gorte, R.J. and J.M. Vohs. (2010). "Substrate-Mediated Spreading and Phase Segregation at LSM-Zirconia Interfaces." *Journal of the Electrochemical Society*. Vol. 158 (2). pp. B79-B83.

# Substrate-Mediated Spreading and Phase Segregation at LSM-Zirconia Interfaces

**Abstract**
Atomic force microscopy and electron microscopy with energy dispersive X-ray analysis was used to characterize changes in teh structure and composition of $La_{0.8}Sr_{0.2}MnO_3$ (LSM) nanoparticles supported on single crystal YSZ (100) (yttria-stabilized zirconia) and $SrTiO_3$(100) surfaces as a function of temperature and exposure to oxidizing and reducing environments. On YSZ(100), LSM particles were found to decompose into Mn- and La-rich phases and spread over the surface upon calcination in air at temperatures above 1123 K. The Mn-rich phase was observed to have a higher mobility and spread more rapidly. In contrast to YSZ(100), on $SrTiO_3$(100) the LSM particles underwent agglomeration via an Ostwald ripening mechanism upon calcination at temperatures above 1123 K, resulting in an increase in the particle size. Phase separation was not observed on this substrate.

**Disciplines**
Biochemical and Biomolecular Engineering | Chemical Engineering | Engineering

**Comments**
Suggested Citation:
Kim, J.S., Lee, S., Gorte, R.J. and J.M. Vohs. (2010). "Substrate-Mediated Spreading and Phase Segregation at LSM-Zirconia Interfaces." *Journal of the Electrochemical Society.* Vol. 158 (2). pp. B79-B83.

*Journal of The Electrochemical Society*, **158** (2) B79-B83 (2011)
0013-4651/2010/158(2)/B79/5/$28.00 © The Electrochemical Society


# Substrate-Mediated Spreading and Phase Segregation at LSM-Zirconia Interfaces

**Ju-Sik Kim, Shiwoo Lee,* Raymond J. Gorte,* and John M. Vohs*,z**

*Department of Chemical and Biomolecular Engineering, University of Pennsylvania, Philadelphia, Pennsylvania 19104, USA*

Atomic force microscopy and electron microscopy with energy dispersive X-ray analysis was used to characterize changes in the structure and composition of $La_{0.8}Sr_{0.2}MnO_3$ (LSM) nanoparticles supported on single crystal YSZ(100) (yttria-stabilized zirconia) and $SrTiO_3$(100) surfaces as a function of temperature and exposure to oxidizing and reducing environments. On YSZ(100), LSM particles were found to decompose into Mn- and La-rich phases and spread over the surface upon calcination in air at temperatures above 1123 K. The Mn-rich phase was observed to have a higher mobility and spread more rapidly. In contrast to YSZ(100), on $SrTiO_3$(100) the LSM particles underwent agglomeration via an Ostwald ripening mechanism upon calcination at temperatures above 1123 K, resulting in an increase in the particle size. Phase separation was not observed on this substrate.
 [DOI: 10.1149/1.3507286] 

Manuscript submitted July 7, 2010; revised manuscript received October 5, 2010. Published November 30, 2010.

Solid oxide fuel cells (SOFC) and solid oxide electrolysis cells (SOE) are promising technologies for the efficient interconversion of chemical and electrical energies. These devices typically use yttria-stabilized zirconia (YSZ) as an oxygen ion conducting electrolyte and operate at temperatures in excess of 923 K. The air electrodes in these systems are generally composed of a porous composite of the YSZ electrolyte and an electronic or mixed electronic/ionic conducting perovskite oxide with strontium-doped lanthanum manganate, $La_{0.8}Sr_{0.2}MnO_3$ (LSM), being the most common. The structural and chemical properties of the interfaces between the electronically conducting perovskite and the YSZ electrolyte are critical in determining the performance of the electrode. For LSM, which has very low ionic conductivity, this is especially true because the electrochemical reactions likely occur only at three-phase boundary (TPB) sites, i.e., the locus of sites at the exposed interface between the electrolyte, the LSM, and the gas phase. The performance of LSM–YSZ composite electrodes is, therefore, highly dependent on the local structure and composition at the interface, which can be a function of the synthesis and operating conditions.[1-9] An important example of this is the observation that the area specific resistance (ASR) of LSM–YSZ electrodes often decreases dramatically when they are cathodically polarized.[5,10-14] This phenomenon, which is referred to as activation polarization, is reversible upon anodic polarization[12,14] or annealing in air at open circuit. A variety of mechanisms for activation polarization have been proposed[10,12,14] including Sr segregation within the LSM[10,13] and morphological changes in the LSM resulting from changes in $P_{O_2}$.[8,12,14,15]

Understanding the effects that LSM–YSZ interactions have on the structure and performance of cathodes and the causes for activation polarization have motivated a number of previous studies of the dynamics of model LSM–YSZ interfaces.[8,15-18] For example, our group has previously investigated how changes in sintering temperature and $P_{O_2}$ affect the structure of LSM nanoparticles supported on a YSZ(100) single crystal surface.[8,9,15] In this work atomic force microscopy (AFM) images showed that the supported LSM nanoparticles spread over the YSZ(100) surface upon annealing in air at temperatures above 1273 K. The spreading was reversed, however, when the sample was annealed in $H_2$ at 973 K, conditions that simulate high cathodic overpotentials. This treatment resulted in the reappearance of a distribution of LSM nanoparticles on the YSZ(100) surface. Based on these results it was argued that the decrease in the ASR of LSM–YSZ cathodes that occurs upon cathodic polarization is caused by the breakup of the dense LSM coating that is formed on the YSZ during the high-temperature synthesis steps, resulting in an increase in the TPB area. Several subsequent studies have provided additional evidence to support this mechanism.[14,16] For example, la O' et al. have reported that cathodic polarization caused a 65 nm thick, dense, LSM film on a planar YSZ support to break up into nanoparticles.[16] A study from our laboratory has also shown that LSM–YSZ electrodes that consist of a high surface-area, LSM nanoparticle coating on the YSZ does not exhibit polarization activation.[7] These electrodes were synthesized by infiltrating the LSM into a porous YSZ scaffold, thereby avoiding high-temperature (>1273 K) annealing steps that tend to produce a dense LSM film.

While the results described above provide strong evidence that structural modification of the LSM plays an important role in the mechanism of activation polarization, there is also some evidence that ion segregation[19,20] and/or phase separation[21] may play a role. For example, Fister et al. used synchrotron-based total reflection X-ray fluorescence measurements to monitor the spatial variations in the composition of $La_{0.7}Sr_{0.3}MnO_3$ (001)-oriented single crystal thin films as a function of $P_{O_2}$ and observed segregation of Sr to the surface of the film at low $P_{O_2}$ ($<10^{-1}$ atm).[19] This process was reversible and Sr-enrichment of the surface was eliminated upon the application of higher $P_{O_2}$. Backhaus-Ricoult et al. have also observed via in situ photoelectron spectroscopy that Mn ions spread away from the LSM–YSZ TPB and over the YSZ surface under cathodic polarization.[17] This process was found to be reversed upon anodic polarization. These results suggest that decomposition of the LSM and the spreading of $MnO_x$ films on the YSZ surface may play a role in the polarization-dependent properties of the LSM.

In this study we have further examined how temperature and $P_{O_2}$ affect the sintering behavior and the structure and composition of LSM particles in contact with YSZ. AFM and secondary electron microscopy (SEM) were used to characterize the structure of model LSM–YSZ(100) interfaces as a function of temperature and $P_{O_2}$. Of particular interest in this work was to evaluate whether the $P_{O_2}$-dependent morphological changes in YSZ-supported LSM particles observed in our previous studies are accompanied by changes in the composition of the YSZ and the possible role that the formation of $MnO_x$ films on the YSZ surface, as suggested by Backhaus-Ricoult et al., may play in directing the observed morphological changes.

## Experimental

LSM powder was synthesized using the Pechini method. An aqueous solution containing stoichiometric quantities of the nitrate salts of the constituent metal ions and an amount of citric acid equal to that of the metal ions was evaporated, and the resulting powder was calcined at 1473 K for 4 h. The LSM powder was then sonicated in a mixture of distilled water and ethanol for 1 h using an ultrasonic cell disruptor in order to break up agglomerates and form

* Electrochemical Society Active Member.
z E-mail: vohs@seas.upenn.edu

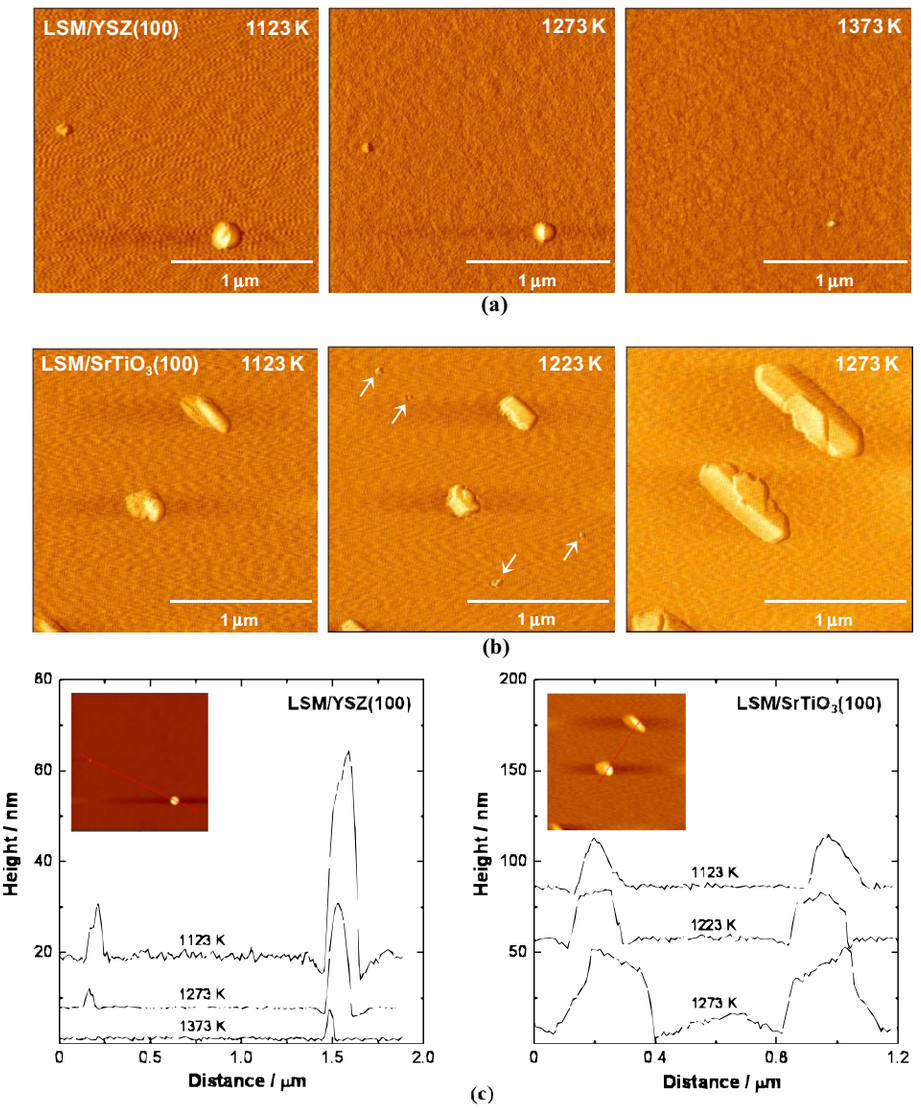


**Figure 1.** (Color online) 2 μm × 2 μm AFM images of LSM nanoparticles on (a) YSZ(100) and (b) $SrTiO_3$(100) single crystals obtained after annealing in air at the indicated temperatures. (c) Line scans obtained from each image.

nanoparticles. After allowing the solutions to settle, the fine particles that remained in solution were extracted and then suspended in water. $La_2O_3$ and $Mn_2O_3$ (Alfa Aesar, ACS 99.9%) particle suspensions were prepared in a similar manner.

An air brush was used to deposit the particle suspensions onto 10 × 10 × 0.5 mm single crystal, YSZ(100) and $SrTiO_3$(100) substrates (MTI Corporation). During deposition, the substrates were heated to 393 K to evaporate the water. Samples were subsequently annealed for 4 h at 1123, 1273, and 1373 K using ramp-up and cool-down rates of 2°C/min.

AFM was performed under ambient conditions on a commercial Pacific Nanotechnology microscope and used n-doped silicon probes with tip radii between 10 and 15 nm. Fiducial marks were placed on the sample using a nanoindenter to allow the same regions to be characterized after heat-treatment. AFM images were taken at least 500 μm away from the nanoindentations. Nanorule software (Pacific Nanotechnology Inc.) was used for particle analysis. Scanning electron microscopy (SEM) with energy dispersive X-ray spectroscopy (EDX) analysis was used to characterize the chemical composition of individual nanoparticles. An electron beam voltage of 15 keV was used during these measurements.

## Results and Discussion

Figure 1a displays a series of AFM images for LSM nanoparticles on YSZ(100) after heating in air for 4 h at 1123, 1273, and 1373 K. These temperatures were chosen because 1123–1273 K is the typical temperature range for SOFC operation and 1373 K is at the lower end of the temperature range used during electrode fabrication. Note that the same 2μ × 2μ region of the surface is shown in each image. For comparison purposes, an analogous set of data for LSM nanoparticles on $SrTiO_3$(100) are shown Fig. 1b. The maximum temperature in this series was limited to 1273 K due to the fact that restructuring of the $SrTiO_3$(100) surface occurred at higher temperatures. This restructuring produced a very rough surface on which the LSM nanoparticles could not be identified. Figure 1c displays line scans that include the two largest particles in each image. While only very small regions of each surface are shown here, multiple regions were analyzed and consistent results were obtained in each region.

The results for the LSM on the YSZ(100) in Fig. 1a are consistent with our previous study[12] and show two LSM particles that decrease in lateral size and height with increasing calcination temperature. The larger particle in this set of images had an initial

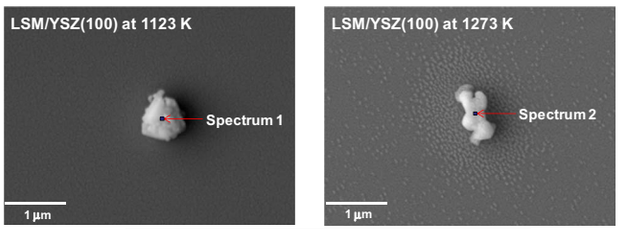


| | atomic percent, % | | | |
|---|---|---|---|---|
| | La | Sr | Mn | O |
| Spectrum 1 (YSZ at 1123 K) | 13.87 | 1.05 | 14.81 | 59.07 |
| Spectrum 2 (YSZ at 1273 K) | 3.36 | 0.00 | 0.00 | 65.39 |

**Figure 2.** (Color online) SEM images of the LSM nanoparticles supported on YSZ(100) single crystal after annealing at 1123 and 1273 K, and the surface composition of the central particle as determined by EDX analysis.

height of 45 nm which decreased to less than 5 nm after heating to 1373 K. Based on similar results in our previous studies, including AFM images collected at higher resolution,[8] it can be inferred that the LSM spreads over the surface of the single crystal YSZ to form a film upon heating above 1300 K. Note that this process occurs well below the melting temperature of the LSM, ~2300 K. In our previous studies[15] we have also shown that the LSM film reagglomerates into particles upon exposure to reducing conditions at high temperature. The spreading of one oxide on the surface of another at temperatures well below the melting temperature of the spreading component is not unusual and has been observed for other systems, such as $V_2O_5$ on $TiO_2$.[22,23] Indeed these wetting phenomena are used in the synthesis of monolayer, metal-oxide, selective-oxidation catalysts.[24] The general rule of thumb is that the ions in the supported oxide will have sufficient mobility to migrate over the surface of the support at temperatures greater than the Tammann temperature ($T_{Tamm} \approx 0.5T_{melt}$). This rule appears to apply to the LSM–YSZ system because spreading of the LSM or its constituent ions was observed to commence near 1273 K which is only slightly greater than the estimated Tammann temperature of 1150 K for LSM.

It is useful to compare the AFM results obtained from LSM/YSZ(100) with those obtained in a similar set of experiments for LSM particles on $SrTiO_3$(100) displayed in Fig. 1b. In this case, spreading of the LSM is not observed; rather the LSM particles agglomerate and increase in size with increasing temperature. The largest particle in this scan region had dimensions of 29 nm × 226 nm × 225 nm after heating to 1123 K, and these increased to 47 nm × 300 nm × 742 nm after heating to 1273 K. This process appears to occur via Ostwald ripening[25,26] in which small LSM particles or clusters migrate across the surface until they attach to a larger particle. The driving force for this process is minimization of the surface free energy of the particles, and it would be expected to occur for the systems in which there are relatively weak interactions between the two oxides. Evidence for this mechanism is provided by the image at 1223 K which contains several very small particles (indicated by arrows in the image) which are not present in the image at 1123 K. The differences in the dynamics of the LSM particles on the YSZ(100) and $SrTiO_3$(100) upon annealing in air, i.e., spreading versus agglomeration, indicate that there must be relatively strong interactions between the LSM (or its constituent ions) and the YSZ.

To provide additional insight into the mechanism of the spreading of the LSM on the YSZ surface under oxidizing conditions, SEM images were obtained, along with EDX analysis of the particle compositions, for samples similar to those in Fig. 1a. Figure 2 displays SEM images of representative supported LSM particles after annealing in air for 4 h at 1123 and 1273 K. In order to facilitate SEM analysis, the samples had to be sputter coated with Au. Figure 2 also shows compositional data obtained by EDX for the LSM particle in each image. The reported compositions were calculated excluding Au, Y, Zr, and other impurities at concentrations below 5 wt %. The image of the sample annealed at 1173 K contains a single LSM particle supported on the smooth YSZ(100) surface. The EDX analysis of this particle shows that, within experimental uncertainty, its composition is consistent with that of the as-deposited particles. Several changes were apparent when the sample was annealed in air at 1273 K, the most noticeable being that the large central particle is now surrounded by a ring of much smaller particles. The density of these particles decreases with increasing lateral distance from the large central particle, suggesting the formation of a film that is spreading away from the LSM particle. Thus, the SEM images are consistent with the AFM data which also suggested the spreading of the LSM particles on YSZ(100) upon heating in air at temperatures above 1200 K.

The EDX analysis of the sample heated to 1273 K is also informative. As shown in Fig. 2, the EDX spectrum obtained from the central, large particle in the image has a substantially different composition than that of the as-deposited LSM particles. Only La and O peaks were detected for this particle, suggesting that it is primarily $La_2O_3$. Due to the relatively low Sr signal in the initial particles, the possibility that the annealed particle contains some Sr cannot be ruled out. EDX spectra were also collected in regions containing the small particles that appear to be spreading away from the central particle. The spectra in this region, however, contained peaks for Y, Zr, and O with only trace amounts of other elements being detected. It appears that the small particles in this region are very thin and that their composition is below the EDX detection limits.

While the EDX results do not provide a direct measure of the composition of the small particles, the fact that the large particle is composed of a La-rich oxide suggests that the small particles are composed of a Mn-rich phase. These results, therefore, suggest that the spreading of the LSM on the YSZ(100) surface that occurs upon annealing in air at temperatures greater than 1200 K (see Fig. 2) involves decomposition of the LSM into La- and Mn-rich phases, with the Mn-rich phase having a higher mobility. To provide additional evidence to support this conclusion, AFM images of $La_2O_3$ and $Mn_2O_3$ particles supported on YSZ(100) were obtained as a function of the annealing temperature in air (Fig. 3 and 4). Similar to the LSM particles on YSZ(100) shown in Fig. 1a, the AFM images

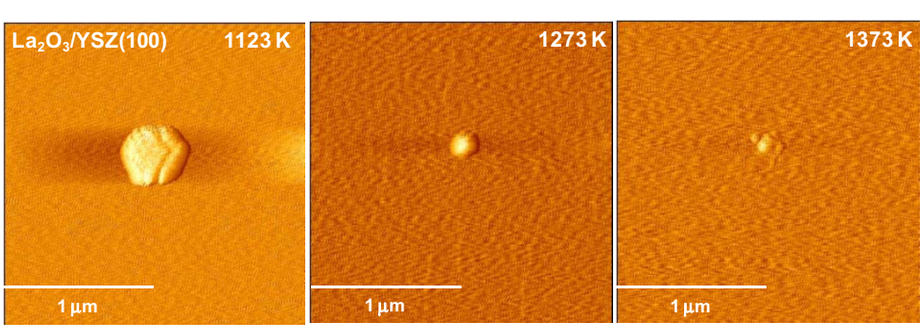


**Figure 3.** (Color online) 2 μm × 2 μm AFM images of a $La_2O_3$ particle on YSZ(100) obtained after annealing in air at the indicated temperatures.

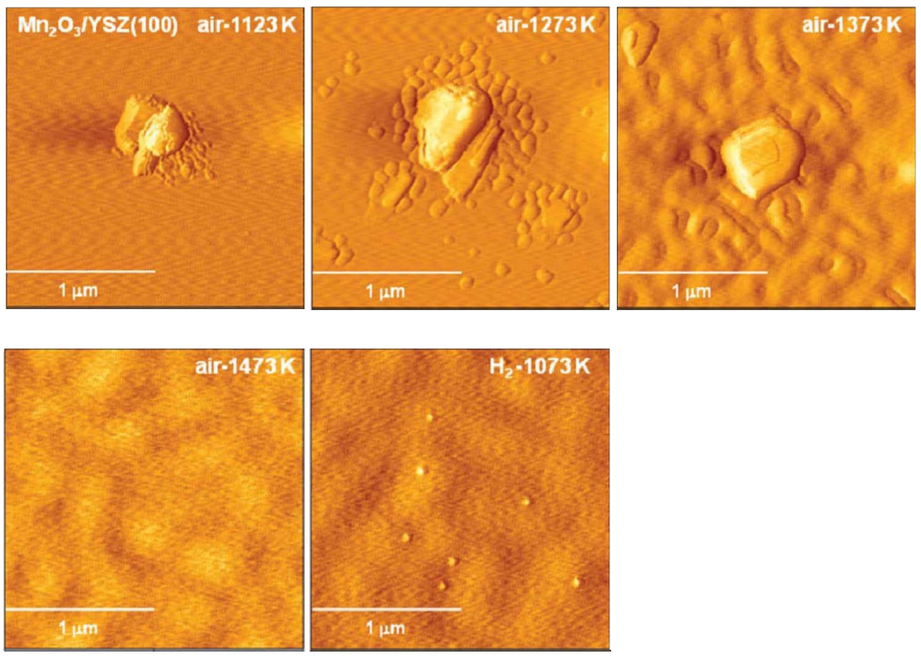


**Figure 4.** (Color online) 2 μm × 2 μm AFM images of a $Mn_2O_3$ particle on YSZ(100) obtained after annealing in air at the indicated temperatures. The final image in the sequence was obtained after heating the sample that had previously been heated in air at 1473 K to 1073 K in $H_2$ (3% $H_2O$) for 16 h.

in Fig. 3 show that $La_2O_3$ particles on this surface also decrease in size with increasing temperature. Because the solubility of La in YSZ is very low[27,28] and the reaction of lanthana with YSZ to form $La_2Zr_2O_7$ only occurs at temperatures above 1373 K,[28] these data suggest that the $La_2O_3$ particles also spread over the YSZ surface at temperatures between 1123 and 1373 K. Following the oxidation treatments, the sample was reduced in $H_2$ (3% $H_2O$) for 16 h at 1073 K; but this was found to produce essentially no changes in the surface morphology.

As shown in Fig. 4, more interesting results were obtained for the $Mn_2O_3$ particles on YSZ(100). The image obtained after annealing in air at 1123 K contains a large $Mn_2O_3$ particle ~200 nm in height that is surrounded by a few smaller particles. After heating to 1273 K, a much higher number of smaller particles appear to be radiating away from the original particle. These satellite particles were relatively uniform in size with a height of ~20 nm. It is noteworthy that the size and distribution of these satellite particles are similar to those in the SEM image of the LSM/YSZ(100) sample annealed at 1273 K, suggesting that the two images are showing the same phenomena. Annealing in air at 1373 K caused significant changes in the morphology of the smaller particles. The observed structural changes imply either formation of a more continuous film of $Mn_2O_3$ or that the $Mn_2O_3$ particles are reacting with the YSZ surface. Unlike $La^{+3}$ and $Sr^{+2}$ ions which have little to no solubility in YSZ,[28-30] thermodynamic calculations indicate that Mn has a solubility of 5.1% in YSZ at 1273 K.[28,29] This supports the latter explanation and indicates that the Mn ions are being incorporated into the near surface region of the YSZ. Further heating to 1473 K caused the disappearance of discrete $Mn_2O_3$ particles, although the YSZ(100) surface is now much more textured compared to that after annealing at lower temperatures. The EDX spectra obtained from the 1473 K heated sample contained peaks only for Y, Zr, and O. This again suggests that the some of the Mn may have dissolved into the YSZ.

The spreading and subsequent dissolution of the Mn into the YSZ were found to be reversible upon treatment under reducing conditions. As shown in Fig. 4, heating the sample that had previously been calcined in air at 1073 to 1473 K in $H_2$ (3% $H_2O$) for 16 h resulted in the reappearance of nanoparticles on the surface. These nanoparticles had no spatial relationship to the small particles observed in the sample annealed at 1273 K. The nanoparticles that reappeared after reduction are most likely composed of MnO, rather than $Mn_2O_3$, due to the highly reducing conditions. It is also noteworthy that the size and distribution of the particles are nearly identical to those observed by Woo et al.[15] for an LSM nanoparticle-YSZ(100) sample that had been annealed in air at 1523 K (i.e., a sample for which the LSM particles have either spread or dissolved into the YSZ), followed by heating in $H_2$ (3% $H_2O$) at 973 K. This similarity suggests that in the case of the air annealed LSM–YSZ(100) sample, the particles that appeared upon reduction were also composed of MnO.

Figure 5 shows a schematic of the processes that were observed to occur upon annealing LSM particles on YSZ(100) in air, followed by subsequent reduction in $H_2$. Upon annealing in air at temperatures above 1200 K, individual LSM particles flatten and appear to spread across the YSZ(100) surface. This process is accompanied by (or perhaps facilitated by) partial decomposition of the LSM and the production of a highly mobile Mn-rich oxide phase that rapidly spreads across the YSZ surface. This spreading process is at least partially reversible and particles are reformed upon exposure to re-

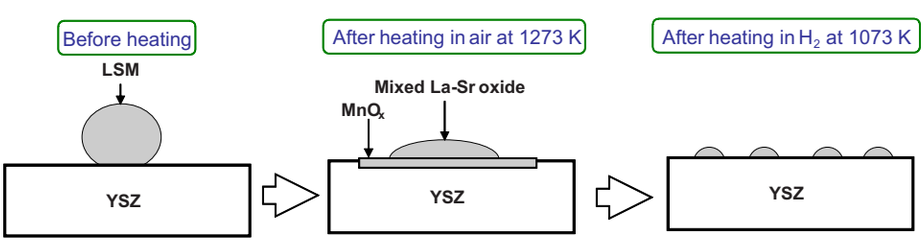


**Figure 5.** (Color online) Schematic diagram of LSM nanoparticles on YSZ(100) single crystals after heating in air at 1273 K, followed by reduction in $H_2/H_2O$ at 1073 K.

ducing conditions at temperatures above 1000 K. In contrast to LSM–YSZ(100), LSM particles on $SrTiO_3(100)$ were more thermally stable and agglomerated into larger particles upon annealing above 1200 K. This difference between the two supports indicates that in the case of LSM–YSZ(100), the driving forces for the morphological and chemical changes in the supported LSM particles must be $P_{O_2}$-dependent interactions between the LSM and its constituent ions and the YSZ surface.

The morphological changes observed for LSM particles supported on YSZ(100) as a function of $P_{O_2}$ occur at temperatures that are typically encountered during the fabrication and operation of SOFC and SOE. As suggested previously,[8-15] these structural changes may play a role in determining the performance of LSM–YSZ composites. For example, the spreading of the LSM on the YSZ at temperatures above 1200 K may lead to the formation of a dense LSM coating over the YSZ during electrode synthesis which typically involves temperatures above 1350 K. This would tend to reduce the number of TPB sites and produce electrodes with relatively poor performance, especially because LSM has very low ionic conductivity. The results obtained in the present study also indicate that this spreading phenomenon may involve the formation of Mn- and La-rich oxide phases with different mobilities. The resulting phase separation near TPB sites would also be expected to alter the electrochemical performance of the electrode. Reagglomeration of the films into particles, which was observed to occur upon exposure to reducing conditions that simulate high cathodic overpotentials, would also be expected to alter electrode performance. In real electrodes, this process might facilitate the break up of dense LSM coatings on the YSZ surface, resulting in an increase in the number of TPB sites.

Finally, the observation that the LSM particles decompose into La-rich and Mn-rich oxide phases, with the latter having a higher mobility on the YSZ(100) surface, is similar to that obtained in the study by Backhaus-Ricoult et al.[17] who also observed the spreading of Mn ions away from an LSM–YSZ interface. The conditions for which $MnO_x$ spreading occurred were quite different in the two studies, however, with spreading observed for oxidizing conditions in the present study and reducing conditions in the Backhaus-Ricoult et al. study. The origin of this discrepancy is not clear but may be related to different treatment conditions and substrates (polycrystalline versus single crystalline) used in each study. It is also possible that the effects observed here may be crystal plane dependent and studies of the dynamics of LSM nanoparticles on other YSZ surfaces [e.g., (111) and (110)] are ongoing.

## Conclusions

The AFM and SEM/EDX data obtained in this study indicate that under oxidizing conditions at temperatures above 1123 K, LSM nanoparticles on YSZ(100) decompose into Mn-rich and La-rich oxide phases that spread over the surface, with the Mn-rich phase having a higher mobility. Reagglomeration of the oxide films formed in this manner was found to occur upon heating under reducing conditions at temperatures. In contrast to YSZ(100), LSM nanoparticles on $SrTiO_3(100)$ interacted weakly with this surface and underwent Ostwald ripening to produce larger particles. The differences in the dynamics of LSM particles on these two substrates indicate that in the case of LSM/YSZ(100), phase separation and spreading of the LSM are mediated by the interactions at the LSM–YSZ interface, including selective dissolution of Mn into the YSZ.

## Acknowledgments

This work was funded by the U.S. National Science Foundation's MRSEC program, grant no. DMR05-20020.

*University of Pennsylvania assisted in meeting the publication costs of this article.*

## References

1. B. C. H. Steele, K. M. Hori, and S. Uchino, *Solid State Ionics*, **135**, 445 (2000).
2. A. V. Virkar, J. Chen, C. W. Tanner, and J. W. Kim, *Solid State Ionics*, **131**, 189 (2000).
3. M. J. Jorgensen, S. Primdahl, C. Bagger, and M. Mogensen, *Solid State Ionics*, **139**, 1 (2001).
4. S. B. Adler, *Chem. Rev.*, **104**, 4791 (2004).
5. S. McIntosh, S. B. Adler, J. M. Vohs, and R. J. Gorte, *Electrochem. Solid-State Lett.*, **7**, A111 (2004).
6. V. A. C. Haanappel, J. Mertens, D. Rutenbeck, C. Tropartz, W. Herzhof, D. Sebold, and F. Tietz, *J. Power Sources*, **141**, 216 (2005).
7. Y. Y. Huang, J. M. Vohs, and R. J. Gorte, *J. Electrochem. Soc.*, **152**, A1347 (2005).
8. Y. Y. Huang, J. M. Vohs, and R. J. Gorte, *Electrochem. Solid-State Lett.*, **9**, A237 (2006).
9. J. M. Vohs and R. J. Gorte, *Adv. Mater.*, **21**, 943 (2009).
10. S. P. Jiang and J. G. Love, *Solid State Ionics*, **138**, 183 (2001).
11. S. P. Jiang and J. G. Love, *Solid State Ionics*, **158**, 45 (2003).
12. S. P. Jiang, *J. Solid State Electrochem.*, **11**, 93 (2006).
13. N. Caillol, M. Pijolat, and E. Siebert, *Appl. Surf. Sci.*, **253**, 4641 (2007).
14. M. A. Haider and S. McIntosh, *J. Electrochem. Soc.*, **156**, B1369 (2009).
15. L. Y. Woo, R. S. Glass, and R. J. Gorte, *J. Electrochem. Soc.*, **156**, B602 (2009).
16. G. J. la O', R. F. Savinell, and Y. Shao-Horn, *J. Electrochem. Soc.*, **156**, B771 (2009).
17. M. Backhaus-Ricoult, K. Adib, T. St. Clair, B. Luerssen, L. Gregoratti, and A. Barinov, *Solid State Ionics*, **179**, 891 (2008).
18. J. Nielsen and T. Jacobsen, *Solid State Ionics*, **179**, 1314 (2008).
19. T. T. Fister, D. D. Fong, J. A. Eastman, P. M. Baldo, M. J. Highland, P. H. Fuoss, K. R. Balasubramaniam, J. C. Meador, and P. A. Salvador, *Appl. Phys. Lett.*, **93**, 151904 (2008).
20. K. Katsiev, B. Yildiz, K. Balasubramaniam, and P. A. Salvador, *Appl. Phys. Lett.*, **95**, 092106 (2009).
21. Y. L. Liu, A. Hagen, R. Barfod, M. Chen, H. J. Wang, F. W. Poulsen, and P. V. Hendriken, *Solid State Ionics*, **180**, 1298 (2009).
22. J. Haber, T. Machej, and T. Czeppe, *Surf. Sci.*, **151**, 301 (1985).
23. J. S. da Cruz, M. A. Fraga, S. Braun, and L. G. Appel, *Appl. Surf. Sci.*, **253**, 3160 (2007).
24. H. Knozinger and E. Taglauer, *Toward Supported Oxide Catalysts via Solid-Solid Wetting*, in Specialist Periodical Reports, Catalysis, Chap. 1, Royal Society of Chemistry, London (1993).
25. L. Ratke and P. W. Voorhees, *Growth and Coarsening: Ostwald Ripening in Material Processing*, pp. 117–125, Springer, New York (2002).
26. A. K. Datye, Q. Xu, K. C. Kharas, and J. M. McCarty, *Catal. Today*, **111**, 59 (2006).
27. H. Yokokawa, N. Sakai, T. Kawada, and M. Dokiya, *J. Electrochem. Soc.*, **138**, 2719 (1991).
28. A. Mitterdorfer and L. J. Gauckler, *Solid State Ionics*, **111**, 185 (1998).
29. H. Yokokawa, *Annu. Rev. Mater. Res.*, **33**, 581 (2003).
30. S. Weber, S. Scherrer, H. Scherrer, M. Kilo, M. A. Taylor, and G. Borchardt, *Appl. Surf. Sci.*, **203–204**, 656 (2003).